RSC Advances

PAPER

View Article Online
View Journal | View Issue

Cite this: *RSC Adv.*, 2018, **8**, 31874

Facile synthesis of size-controlled Fe_2O_3 nanoparticle-decorated carbon nanotubes for highly sensitive H_2S detection†

Wooyoung Kim,[a] Jun Seop Lee *[b] and Jyongsik Jang *[a]

Received 1st August 2018
Accepted 6th September 2018

DOI: 10.1039/c8ra06464d

rsc.li/rsc-advances

Hydrogen sulfide (H_2S) is one of the most plentiful toxic gases in a real-life and causes a collapse of the nervous system and a disturbance of the cellular respiration. Therefore, highly sensitive and selective H_2S gas sensor systems are becoming increasingly important in environmental monitoring and safety. In this report, we suggest the facile synthesis method of the Fe_2O_3 particles uniformly decorated on carbon nanotubes (Fe_2O_3@CNT) to detect H_2S gas using oxidative co-polymerization (pyrrole and 3-carboxylated pyrrole) and heat treatment. The as prepared Fe_2O_3@CNT-based sensor electrode is highly sensitive (as low as 1 ppm), selective and stable to H_2S gas at 25 °C, which shows promise for operating in medical diagnosis and environment monitoring. Excellent performance of the Fe_2O_3@CNT is due to the unique morphology of the nanocomposites made from uniformly dispersed Fe_2O_3 nanoparticles on the carbon surface without aggregation.

1. Introduction

The synthesis of innovative nanomaterials with advanced functions is a continuously expanding issue of materials science.[1–5] On this subject, nanocomposites, consisting of organic and inorganic components, present improved properties originating from each component and satisfy economical and environmental challenges of the industry.[6–8] Metal oxide-containing hybrid carbon nanomaterials are of great interest for diverse applications such as energy storage, catalysis, and sensor device systems.[9–13]

Recently, the concern over the environmental protection and the demand to control hazardous chemicals in industry have caused comprehensive interest in developing sensor systems for various toxic gases.[14–18] Hydrogen sulfide (H_2S), originating from microbial breakdown of plants and animals, is one of the most abundant toxic gases found in coal mines, manholes and semiconducting device industries.[19–23] H_2S is broadly hazardous in the human body causing collapse of the nervous system and disturbance of the cellular respiration due to binding iron in the mitochondrial cytochrome enzymes.[24,25] A threshold limit value (TLV) and recommended acceptable ambient levels of H_2S are, respectively, 10 ppm for 8 h and lower than 0.1 ppm by the Occupational Safety and Health Administration (OSHA).[26] Accordingly, highly sensitive (<10 ppm) and selective detection of H_2S is emerging importance issue in the field of environmental monitoring, disease diagnosis, and food safety. However, conventional H_2S gas sensor has several limitations such as slow response/recovery times and high operating temperature that cause complex sensing platform and lead to difficult placement in the confined area.[27]

Metal oxide semiconductors (MOS) have been conducted in developing H_2S sensor systems due to low operating power, stability, and ease of incorporation into the microelectronic devices.[28–32] Among them, Fe_2O_3 displays critical advantages (*i.e.* ease synthesis, low cost, nontoxicity and abundance in the earth crust) to apply into the H_2S sensor system.[33–36] In spite of these benefits, Fe_2O_3 has several limitations such as a long recovery time and a requirement of heating (200–400 °C) to promote sensing reaction to apply into the real sensing system. Therefore, there are a lot of studies about improving H_2S detecting performance of the Fe_2O_3-based sensor systems through loading with noble metals, doping with catalytic oxides, and composing composites with carbon materials.[37–39] For example, Sun *et al.* fabricated α-Fe_2O_3 nanotubes on the carbon nanotube templates using a hydrothermal synthetic method and a following calcination.[40] Jiang *et al.* synthesized paper like Fe_2O_3/graphene nanosheets by means of a super critical CO_2-assisted thermal process and a controlled magnetic field step.[41] However, it is difficult to control the size of these materials, particularly on the nanoscale; thus, material fabrication process can be very complicated.

[a]*School of Chemical and Biological Engineering, College of Engineering, Seoul National University, 599 Gwanangno, Gwanakgu, Seoul, 151-742 Korea. E-mail: jsjang@plaza.snu.ac.kr; Fax: +82-2-888-1604; Tel: +82-2-880-7069*

[b]*Department of Nanochemistry, College of Bionano, Gachon University, 1342 Seongnamdaero, Sujeong-gu, Seongnam-Si, Gyeonggi-Do, 13120 Korea. E-mail: junseop@gachon.ac.kr; Fax: +82-31-750-5389; Tel: +82-31-750-5814*

† Electronic supplementary information (ESI) available: Raman spectra of nanocomposites; sensing ability of nanocomposites; comparison H_2S sensing performance of different chemical sensors; stability test to H_2S gas. See DOI: 10.1039/c8ra06464d

Herein, we describe a facile synthesis method for Fe_2O_3 particle uniformly decorated carbon nanotubes (Fe_2O_3@CNT) using functional group (–COOH) incorporated polypyrrole nanotubes. First, 3-carboxylated polypyrrole nanotubes (CPPyNT) were fabricated using oxidative co-polymerization between monomers (pyrrole and 3-carboxylated pyrrole) and initiator (iron cation (Fe^{3+}) and methyl orange complex). Then, Fe_2O_3 nanoparticles were formed onto the nanotube structure with phase change of polypyrrole to carbon through simple heat treatment. The Fe_2O_3@CNT was then applied as a hydrogen sulfide (H_2S) gas sensor transducer. The Fe_2O_3@CNT electrode displays enhanced performances (such as rapid response/recovery time, superb cycle stability, low working temperature and highly sensitive to H_2S molecule) than other conventional H_2S sensors owing to uniformly dispersed Fe_2O_3 nanoparticles on the carbon surface. In particular, a minimum detectable level (MDL) of the sensor system is as low as 1 ppm that is much lower than that of other sensors based on Fe_2O_3 contained nanomaterials.[38–42]

2. Experimental section

2.1 Materials

Pyrrole (98%), methyl orange, and iron chloride ($FeCl_3$, 97%) were obtained from Aldrich Co. Pyrrole-3-carboxylic acid was purchased from Acros organics and used without further purification.

2.2 Fabrication of Fe_2O_3@CNT nanocomposites

As a starting material, various carboxylated polypyrrole nanotubes were prepared using a self-degradation method. In detail, a 1.5 mmol of $FeCl_3$ solution was added into 30 ml of 5 mM methyl orange aqueous solution. Then, 2 mmol of pyrrole and pyrrole-3-carboxylic acid mixed monomers were added and stirred at 10 °C for 12 h. Especially the amount of the pyrrole-3-carboxylic acid in the mixed monomers was controlled from 0.2 wt% to 5.0 wt% to form different amount of Fe_2O_3 on the carbon surface. The resulting black precipitate was purified by washing with distilled water several times until the filtrate became transparent. The as prepared black powder was then dried under vacuum at 40 °C for 12 h. Iron oxide (Fe_2O_3) particle decorated carbon nanotubes (Fe_2O_3@CNT) were prepared *via* heating process at 400 °C.

2.3 Characterization

A JEOL 6700 was used to obtain field-emission scanning electron microscope (FE-SEM) images. Transmission electron microscope (TEM) and high-resolution transmission electron microscope (HR-TEM) images were achieved with a JEOL JEM-200CX and JEOL-3010, respectively. X-ray diffraction (XRD) patterns and X-ray photoelectron spectroscopy (XPS) spectra were obtained using the M18XHF SRA (MAC Science Co.) and AXIS-HIS (KRATOS) systems.

2.4 Electrical measurements of the Fe_2O_3@CNT sensor electrode

Fe_2O_3@CNT (0.5 wt% in ethanol solution) was prepared by sonication for deposition onto an as-prepared interdigitated array (IDA) electrode. The as-prepared IDA electrode measured resistance changes in the composites with a source-meter connected to a computer. The Fe_2O_3@CNT sensors were placed in a vacuum chamber with a vapour inlet/outlet pressure of 10^0 torr. Various concentration of H_2S gas (1–100 ppm) was injected into the chamber using a mass flow controller (MFC, KNH Instruments). The real-time responses from the Fe_2O_3@CNT were systematically evaluated by normalized resistance changes. The normalized resistance changes of the Fe_2O_3@CNT based sensor was monitored in a real-time during exposure to various gases at a constant applied current (10^{-6} A) until saturation was reached. After the Fe_2O_3@CNT was exposed to various concentrations of H_2S gas for several minutes, the gas vapour was then replaced by compressed nitrogen gas to remove any molecules attached to the nanomaterials. This process was repeated several times. Vapour/air was supplied at various flow rates ranging from 2 to 8 slm and 1 to 5 sccm, as controlled by the MFC.

3. Results and discussion

3.1 Fabrication of Fe_2O_3@CNT

Fig. 1a suggests the overall procedure for a synthesis of the Fe_2O_3 particle decorated carbon nanotubes (Fe_2O_3@CNT), based on an oxidative co-polymerization process. As a first step material, 3-carboxylated polypyrrole coated nanorod complex was formed by a co-polymerization of monomers (pyrrole and 3-carboxylated pyrrole) and nanorod template (composed of methyl orange and iron chloride). Then, the nanorod template was washed using distilled water to generate 3-carboxylated pyrrole nanotubes (CPPyNT) of *ca.* 100 nm-diameter (Fig. 1b). In particular, iron cations (Fe^{3+}) from the nanorod template are fastened on the nanotube surface because of the covalent bonding between the Fe^{3+} ion and the negative charge of the O atom in the carboxyl group.[43] The CPPyNT was then conducted heat treatment to induce phase transfer of 3-carboxylated polypyrrole to carbon and iron cation (Fe^{3+}) to iron oxide (Fe_2O_3), respectively. Consequently, Fe_2O_3@CNT was formed as shown in Fig. 1C.

During the heating procedure, a carboxyl group (–COOH) acts as a nucleation site to form Fe_2O_3 nanoparticles on the carbon surface. For the without carboxyl group based composites, a small number of Fe_2O_3 particles is randomly decorated on the carbon surface with different sizes from 4 nm to 11 nm (Fig. 2a). On the other hand, a size and a population of the Fe_2O_3 particles are uniformly reduced and enhanced, respectively, with increasing concentration of the carboxyl group on the surface (from 0.2 wt% to 3.0 wt%) due to improve amount of nucleate sites (–COOH) and iron cations (Fe^{3+}). The Fe_2O_3@CNT with 0.2 wt%, 1.0 wt%, and 3.0 wt% carboxyl group concentrations are denoted as Fe_2O_3@CNT_0.2, Fe_2O_3@CNT_1.0, and Fe_2O_3@CNT_3.0. Fig. 2b–d display that an average diameter of

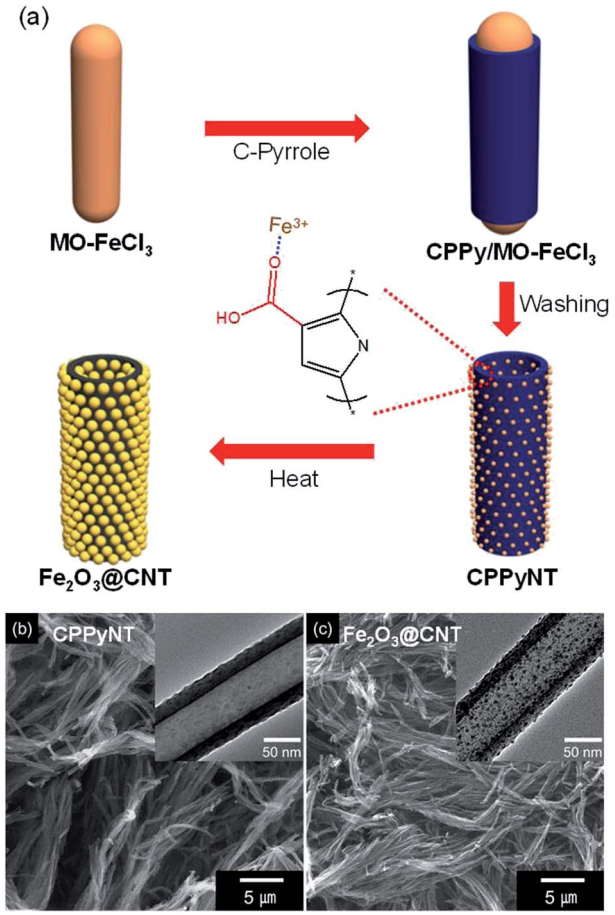

Fig. 1 (a) Illustrative of the sequential synthesis of the iron oxide decorated carbon nanotube composites. Field-emission scanning electron microscopy (FE-SEM) and transmission electron microscopy (TEM) (inset) images of (b) the carboxylated polypyrrole nanotubes (CPPyNT) and (c) the iron oxide decorated carbon nanotubes (Fe_2O_3@CNT).

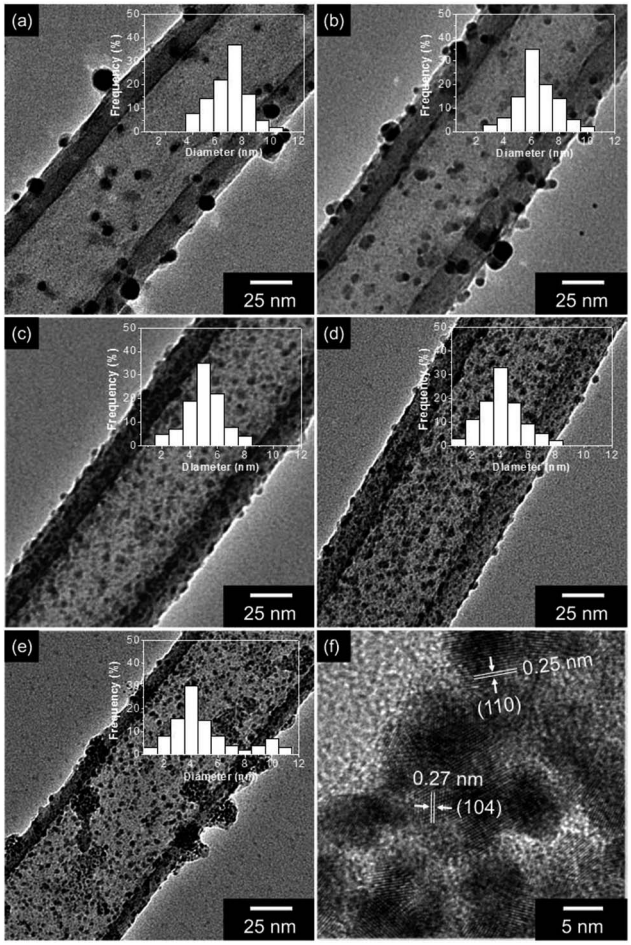

Fig. 2 TEM images and Fe_2O_3 size distributions (inset) of the nanocomposites with different amount of carboxyl group on the polypyrrole surface: (a) without; (b) 0.2 wt%; (c) 1.0 wt%; (d) 3.0 wt%; (e) 5.0 wt%. (f) High-resolution transmission electron microscopy (HR-TEM) image of the Fe_2O_3@CNT with 3.0 wt% of carboxyl group.

the particles decreases from 7 nm (0.2 wt%) to 4 nm (3.0 wt%) and a population of the particles dramatically increases up to 3.0 wt%. However, a diameter of the Fe_2O_3 particles increases from more than 3.0 wt% concentration of a carboxyl group owing to a large amount of iron cations is caused aggregation of the Fe_2O_3 during phase transfer process. Fig. 2e shows Fe_2O_3@CNT at 5.0 wt% of a carboxyl group (denoted as Fe_2O_3@CNT_5.0) contained large diameter (more than 10 nm) of the particles on the surface. In addition, a high resolution transmission microscopy (HR-TEM) image of the particles indicates interlayer spacing of 0.25 nm and 0.27 nm for (110) and (104) of hematite Fe_2O_3 and confirms that α-Fe_2O_3 phase is generated after a heat treatment step (Fig. 2f).

3.2 Characterization of Fe_2O_3@CNT

To confirm crystallinity and chemical composition of the nanocomposites, X-ray diffraction (XRD), Raman and X-ray photoelectron spectroscopy (XPS) are determined as follows. Fig. 3a suggests XRD patterns of the each synthesis state of the nanotubes (CPPyNT and Fe_2O_3@CNT). The peaks of the inorganic materials in the Fe_2O_3@CNT are well matched α-Fe_2O_3 phase (hematite, JCPDS 33-0664), indicating the formation of α-Fe_2O_3 nanoparticles into the carbon structure. However, the broad peaks around 25° are difficult to illustrate phase transform of the CPPy to carbon structure. Therefore, Raman spectroscopy is used to confirm phase change of the CPPy after heat treatment (Fig. S1†). The ratio of D and G peaks (I_G/I_D) is higher for the Fe_2O_3@CNT (*ca.* 1.3) than that for the CPPyNT (*ca.* 0.8), and peaks for Fe_2O_3@CNT are sharper than CPPyNT. Consequently CPPyNT is converted to amorphous carbon with Fe_2O_3 nanoparticle generation through heating process.

Fig. 3b presents complete spectra over the range over of 0–1200 eV. These overview spectra illustrate that the C, N, O and Fe atoms are existed in the Fe_2O_3@CNT, whereas only C, N and O atoms are suggested in the CPPyNT. The peak of N 1s is attributed to nitrogen atoms from the pyrrole component. High-resolution XPS spectra for the C 1s around 285 eV are shown in Fig. 3c; this peak is deconvoluted into four components. The peaks of the CPPyNT are attributed as follows: the 284.3 eV peak

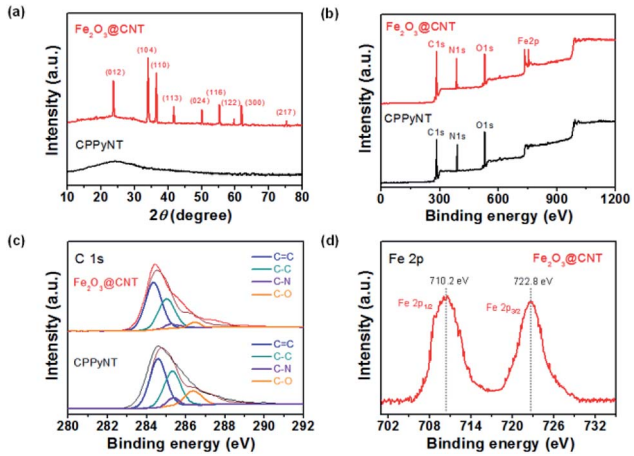

Fig. 3 (a) X-ray diffraction (XRD) spectra and (b) fully scanned X-ray photoelectron spectroscopy (XPS) of the nanotubes. (c) C 1s and (d) Fe 2p XPS spectra of the nanotubes. (black: CPPyNT, red: Fe_2O_3@CNT).

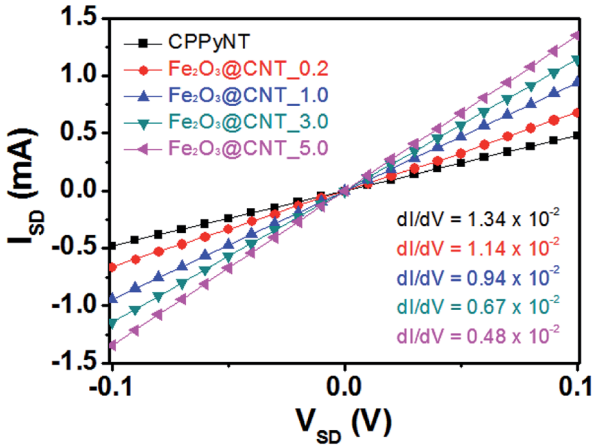

Fig. 4 *I–V* curves of the different nanotubes (black: CPPyNT; red: Fe_2O_3@CNT_0.2; blue: Fe_2O_3@CNT_1.0; green: Fe_2O_3@CNT_3.0; pink: Fe_2O_3@CNT_5.0).

to C=C bonds, the 285.3 eV peak to C–C bonds, the 286.6 eV peak to C–O bonds, and the 284.9 eV peak to C–N bonds. But, Fe_2O_3@CNT suggests increase peak at 284.6 eV, which is attributed to graphitic sp^2 hybridization, and decrease peaks at 285.5 and 287.9 eV, assigned to C–O and C–N, after heat treatment. A high resolution spectrum for the Fe 2p of the Fe_2O_3@CNT is also suggested in Fig. 3d. In the Fe 2p spectrum, spin–orbit components of $2p_{3/2}$ and $2p_{1/2}$ are shown near 710.2 and 722.8 eV, indicating that the valence state of Fe is +3. Consequently, the final product (Fe_2O_3@CNT) is composed of Fe_2O_3 nanoparticle decorated amorphous carbon nanotubes as confirmed by HR-TEM, XRD, and XPS.

3.3 Real-time responses for sensing of H_2S

To characterize electrical properties of the Fe_2O_3@CNT-based sensor device, the composite nanotubes are immobilized on an interdigitated array (IDA) sensor electrode using spin-coating method. Fig. 4 displays linear current–voltage (*I–V*) curves of the various nanotubes for the voltage range from −0.1 to +0.1 V. A linearity of the *I–V* curves indicates that the nanotubes are uniformly immobilized on the sensor electrode with ohmic contact rather than Schottky barriers. In particular, d*I*/d*V* (=1/*R*) value of the electrodes decreases with an increase in the population of the Fe_2O_3 particles on the carbon surface due to high resistive metal oxide semiconductor particles enhancing the resistivity of the nanotube composites.

The uniformly dispersed Fe_2O_3 particles on the carbon surface rapidly detect H_2S gas at room temperature by a chemical reaction between adsorbed oxygen species and H_2S gas (Fig. 5). Sensing mechanism of the Fe_2O_3@CNT is illustrated as below. Initially, an electron depletion layer, composed of negatively charged adsorbing oxygen species (O^{2-}, O^-, and O_2^-), is formed on the Fe_2O_3 particle surface after exposing of the sensor electrode to air.[39] Chemical reactions of adsorbed oxygen species are suggested as follows:

$$O_2(g) \rightarrow O_2(ads) \quad (1)$$

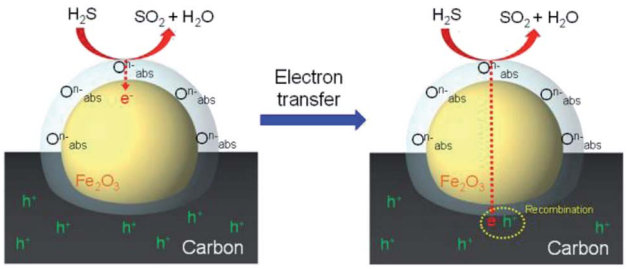

Fig. 5 H_2S gas detection mechanism of the Fe_2O_3@CNT based-sensor electrode at room temperature.

$$O_2(ads) + \alpha e^- \rightarrow O_2^{\alpha-}(ads). \quad (2)$$

When the sensor electrode is exposed to H_2S gas, the chemisorbed oxygen species on the Fe_2O_3 particles oxidize H_2S gas. In detail, the oxygen species dissemble H_2S gas into H_2O and SO_2 gases with transferring electrons to the Fe_2O_3 and the carbon nanotube structure.[39] Oxidation reaction of H_2S gas on the Fe_2O_3 particles is described by

$$2H_2S(g) + 3O_2^{\alpha-}(ads) \rightleftarrows 2H_2O(g) + 2SO_2(g) + 3\alpha e^-. \quad (3)$$

A resistance of the sensor electrode increases with electron transfer due to decrease a population of charge carriers (hole) through recombination of the transferred electron and the hole in the carbon structure. Then, H_2O and SO_2 gases from the oxidation of H_2S are desorbed by exposure air contained gas (N_2 80 vol% and O_2 20 vol%) again. Consequently, the amount of chemisorbed oxygen species on the Fe_2O_3 surface effects on the sensing ability of the sensor electrode. Thus, a large population of the small sized-Fe_2O_3 provides an increase in specific surface area to H_2S gas and efficient electron transfer to the carbon structure.

To investigate the sensing abilities of the Fe_2O_3@CNT-based sensor electrode, real-time responsive resistance changes are evaluated for different concentrations of H_2S gas at room

temperature. Fig. 6a presents a real time response of the sensor electrodes with different amount of Fe_2O_3 decoration as a function of H_2S concentration. Upon various concentrations of H_2S exposure, the Fe_2O_3@CNT based electrodes display a rapid resistance improvement less than 30 s before reaching a saturated value. A minimum detectable level (MDL) of the each electrode presents as following values: 20 ppm for the Fe_2O_3@CNT_0.2; 5 ppm for the Fe_2O_3@CNT_1.0; 1 ppm for the Fe_2O_3@CNT_3.0; 1 ppm for Fe_2O_3@CNT_5.0 (Fig. S2†). The MDL value of the Fe_2O_3@CNT based electrode suggests much lower than that of other conventional Fe_2O_3 sensors at low working temperature (25 °C) (Table S1†). Thus, a better sensitive response is attained concomitant with a high density of the Fe_2O_3 active site that causes enhancement of activity to H_2S gas. However, even though the Fe_2O_3@CNT_5.0 contains more Fe_2O_3 particles than the Fe_2O_3@CNT_3.0, a value of MDL and a sensitive response of the Fe_2O_3@CNT_5.0 are lower than that of the Fe_2O_3@CNT_3.0 because an excess amount of Fe_2O_3 component generates aggregation rather than small particles and then reduces active surface area to H_2S gas. Moreover, the improved active surface area of the Fe_2O_3 particles cause rapid diffusion of H_2S and increase sensitivity with providing more active sites (chemisorbed oxygen species) to detect H_2S.

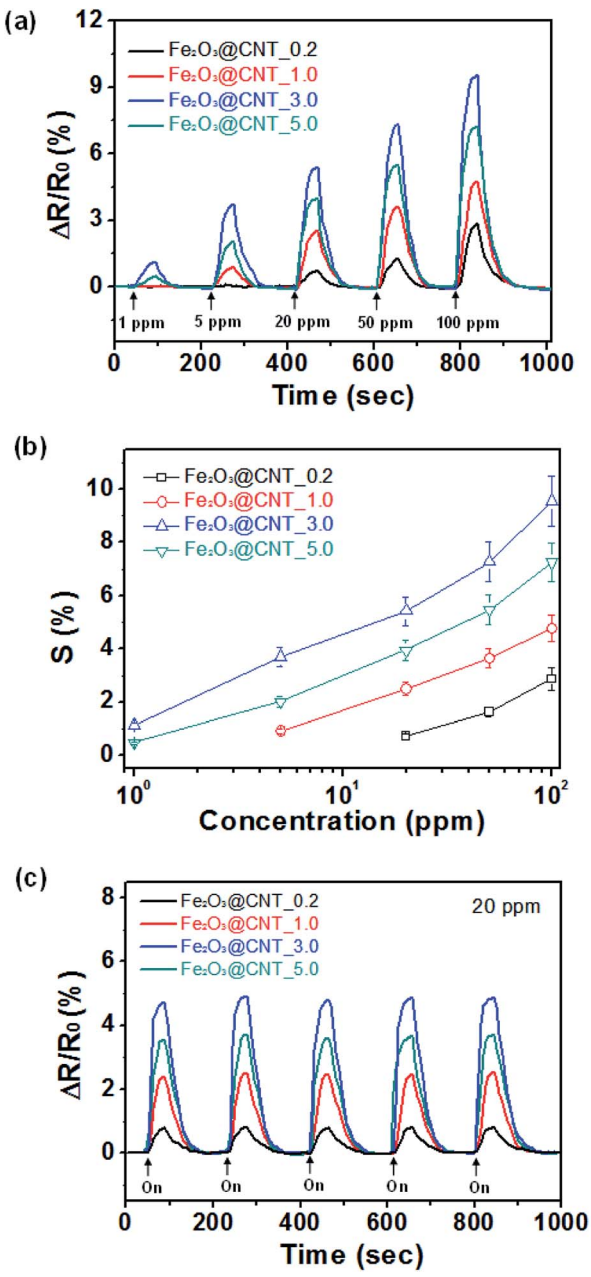

Fig. 6 Reversible and reproducible responses are measured at a current value (10^{-6} A) with the different nanocomposites. (a) Normalized resistance changes upon sequential exposure to various concentrations of H_2S. (b) Sensitivity (S) calibration line as a function of H_2S concentration. (c) Normalized resistance changes of different composites upon sequential periodic exposure to 20 ppm of H_2S gas. (Each nanocomposite represents as following: black: Fe_2O_3@CNT_0.2; red: Fe_2O_3@CNT_1.0; blue: Fe_2O_3@ CNT_3.0; green: Fe_2O_3@CNT_5.0.)

Fig. 6b represents sensitivity changes of the electrode as a function of an amount of Fe_2O_3 particles, with respect to H_2S concentration. The sensitivity (S) is determined from the saturation point of the normalized resistance change after 30 s of H_2S exposure. As lower than 1 ppm, the sensor electrodes present nonlinear changes in sensitivity. On the other hand, linear tendency is observed over a wide range of H_2S concentration (from 1 ppm to 100 ppm). Accordingly, the Fe_2O_3@CNT based sensor electrodes illustrate reversible and reproducible responses to various concentration of the target analyte (H_2S), and sensing ability is more pronounced as enhancing concentration of the analyte.

To apply practical application into the sensor systems, splendid cycle stability is desired for sensor transducer materials. Fig. 6c shows the electrical responses of the sensor electrodes upon periodic disclosure to 20 ppm of H_2S at room temperature. The different Fe_2O_3@CNT nanotubes show similar responses for an each time without retardation of the response and recovery times owing to small size of the Fe_2O_3 nanoparticles transfer electrons quickly and generate the uniform electron depletion layer on the surface. Moreover, sensing ability of the Fe_2O_3@CNT sensor electrode also remains sensitivity more than 95% of initial value after 4 weeks that is higher than that of other conventional metal oxide based sensor electrode (Fig. S3†).[19–23] Therefore, the Fe_2O_3@CNT based sensor electrode suggests high stability to H_2S gas detection.

The selectivity of the sensor electrodes is also one of the important issues to apply them into practical application. In other words, it is essential to specific detect the target analyte among various chemicals. To evaluate selectivity, Fe_2O_3@-CNT_3.0 based electrode is exposed to different reducing (H_2S and NH_3) and oxidizing (NO_2, MeOH and Et–OH) gases at concentrations of 20 ppm. As shown in Fig. 7, the sensor electrode displays much higher response to H_2S than that of other gases due to strong interaction between H_2S and the chemisorbed oxygen species and low bonding energy (381 kJ mol^{-1}) of H_2S.[44] A faster release of trapped electrons in the Fe_2O_3 particles is also one of important constituents of the selectivity. Thus, H_2S can be classified from other chemicals based on the extent and direction of the resistance changes upon analyte disclosures.

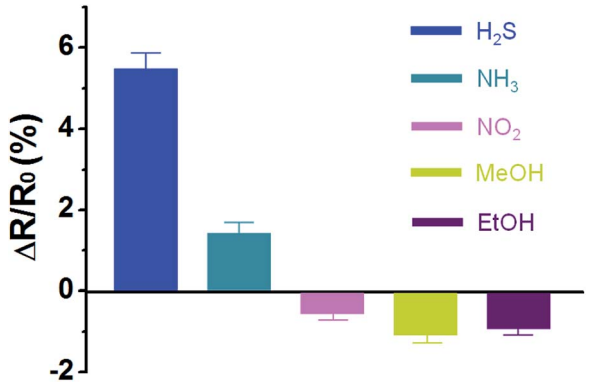

Fig. 7 Normalized resistance changes of Fe_2O_3@CNT_3.0 based sensor electrode to different analytes: concentration of the chemicals is maintained at 20 ppm.

4. Conclusions

In summary, a size and an amount of the Fe_2O_3 decoration controlled carbon nanotubes (Fe_2O_3@CNT) are facilely synthesized using co-polymerization of monomers (pyrrole and 3-carboxylated pyrrole) and following heat process. The Fe_2O_3@CNT is then applied in an ultra-highly sensitive H_2S gas sensor electrode at room temperature. Especially, the uniformly decorated Fe_2O_3 particles conduct critical roles in H_2S sensing system as below: (1) formation of the chemisorbed oxygen species to cause reaction with H_2S molecule; (2) maximize of the active surface area to the target analyte; (3) rapid electron transfer from H_2S to the carbon nanotubes; (4) excellent cycle stability without morphology collapse. As a result, the Fe_2O_3@CNT sensor presents excellent cycle stability, selectivity, and highly sensitive (1 ppm of minimum detectable level) to H_2S gas at room temperature that is much higher performative than other sensor electrodes based on Fe_2O_3 included nanomaterials.[38–42] Therefore, this work suggests a facile synthesis of metal oxide/carbon nanocomposites for various applications such as energy storage electrode, electrochemical catalyst and sensor electrode.

Conflicts of interest

There are no conflicts to declare.

Notes and references

1 N. Saraf, E. R. Woods, M. Peppler and S. Seal, *Biosens. Bioelectron.*, 2018, **117**, 40–46.
2 Y. Koskun, A. Savk, B. Sen and F. Sen, *Anal. Chim. Acta*, 2018, **1010**, 37–43.
3 Q. Hu, Q. Wang, C. Jiang, J. Zhang, J. Kong and X. Zhang, *Biosens. Bioelectron.*, 2018, **110**, 52–57.
4 S. Bozkurt, B. Tosun, B. Sen, S. Akocak, A. Savk, M. F. Ebeoglugil and F. Sen, *Anal. Chim. Acta*, 2017, **989**, 88–94.
5 G. Baskaya, Y. Yildiz, A. Savk, T. O. Okyay, S. Eris, H. Sert and F. Sen, *Biosens. Bioelectron.*, 2017, **91**, 728–733.
6 L. Gong, I. A. Kinloch, R. J. Young, I. Riaz, R. Jalil and K. S. Novoselov, *Adv. Mater.*, 2010, **22**, 2694–2697.
7 M. R. Gholipour, C.-T. Dinh, F. Beland and T.-O. Do, *Nanoscale*, 2015, **7**, 8187–8208.
8 M. Kruk and M. Jaroniec, *Chem. Mater.*, 2001, **13**, 3169–3183.
9 G. Li, J. Zhang, W. Li, K. Fan and C. Xu, *Nanoscale*, 2018, **10**, 9252–9260.
10 J. S. Lee, D. H. Shin and J. Jang, *Energy Environ. Sci.*, 2018, **8**, 3030–3039.
11 H. Wang, L. Wei, F. Ren, Q. Wang, L. D. Pfefferle, G. L. Haller and Y. Chen, *ACS Nano*, 2013, **7**, 614–626.
12 J. S. Lee, S. G. Kim, S. Cho and J. Jang, *Nanoscale*, 2015, **7**, 20665–20673.
13 J. S. Lee and A. Manthiram, *J. Power Sources*, 2017, **343**, 54–59.
14 Y. Zhao, J.-G. Song, G. H. Ryu, K. Y. Ko, W. J. Woo, Y. Kim, D. Kim, J. H. Lim, S. Lee, Z. Lee, J. Park and H. Kim, *Nanoscale*, 2018, **10**, 9338–9345.
15 J. S. Lee, O. S. Kwon, D. H. Shin and J. Jang, *J. Mater. Chem. A*, 2013, **1**, 9099–9106.
16 Z. Hua, C. Tian, Z. Qiu, Y. Li, X. Tian, M. Wang and E. Li, *Sens. Actuators, B*, 2018, **259**, 250–257.
17 K. J. Dunst, K. Trzcinski, B. Scheibe, M. Sawczak and P. Jasinski, *Sens. Actuators, B*, 2018, **260**, 1025–1033.
18 J. Jun, J. S. Lee, D. H. Shin, J. Oh, W. Kim, W. Na and J. Jang, *J. Mater. Chem. A*, 2017, **5**, 17335–17340.
19 S. Ghosh, D. Adak, R. Bhattacharyya and N. Mukherjee, *ACS Sens.*, 2017, **2**, 1831–1838.
20 J. Shu, Z. Qiu, S. Lv, K. Zhang and D. Tang, *Anal. Chem.*, 2017, **89**, 11135–11142.
21 K. Tian, X.-X. Wang, Z.-Y. Yu, H.-Y. Li and X. Guo, *ACS Appl. Mater. Interfaces*, 2017, **9**, 29669–29676.
22 M. Asad, M. H. Sheikhl, M. Pourfath and M. Moradi, *Sens. Actuators, B*, 2010, **210**, 1–8.
23 P.-G. Su and Y.-T. Peng, *Sens. Actuators, B*, 2014, **193**, 637–643.
24 H. Wu, Z. Chen, J. Zhang, F. Wu, C. He, B. Wang, Y. Wu and Z. Ren, *J. Mater. Chem. A*, 2016, **4**, 1096–1104.
25 A. F. S. Abu-Hani, Y. E. Greish, S. T. Mahmound, F. Awwad and A. I. Ayesh, *Sens. Actuators, B*, 2017, **253**, 677–684.
26 A. B. Bodade, A. M. Bende and G. N. Chaudhari, *Vacuum*, 2008, **82**, 588–593.
27 Q. Li and J. R. Lancaster Jr, *Nitric Oxide*, 2013, **35**, 21–34.
28 C. Wang, X. Chu and M. Wu, *Sens. Actuators, B*, 2006, **113**, 320–323.
29 L. Wang, Y. Kang, Y. Wang, B. Zhu, S. Zhang, W. Huang and S. Wang, *Mater. Sci. Eng., C*, 2012, **32**, 2079–2085.
30 S. M. Kanan, O. M. El-Kadri, I. A. Abu-Yousef and M. C. Kanan, *Sensors*, 2009, **9**, 8158–8196.
31 Y.-F. Sun, S.-B. Liu, F.-L. Meng, J.-Y. Liu, X. Jin, L.-T. Kong and J.-H. Liu, *Sensors*, 2012, **12**, 2610–2631.
32 L. Xu, Z. Dai, G. Duan, L. Guo, Y. Wang, H. Zhou, Y. Liu, W. Cai, Y. Wang and T. Li, *Sci. Rep.*, 2015, **5**, 10507.
33 J. Deng, J. Ma, L. Mei, Y. Tang, Y. Chen, T. Lv, Z. Xu and T. Wang, *J. Mater. Chem. A*, 2013, **1**, 12400–12403.

34 V. Balouria, A. Kumar, A. Samanta, A. Singh, A. K. Debnath, A. Manhajan, R. K. Bedi, D. K. Aswal and S. K. Gupta, *Sens. Actuators, B*, 2013, **181**, 471–478.
35 Y. Wang, F. Kong, B. Zhu, S. Wang, S. Wu and W. Huang, *Mater. Sci. Eng., B*, 2007, **140**, 98–102.
36 H. Kheel, G.-J. Sun, J. K. Lee, S. Lee, R. P. Dwivedi and C. Lee, *Ceram. Int.*, 2016, **42**, 18597–18604.
37 Y. Wang, Y. Wang, J. Cao, F. Kong, H. Xia, J. Zhang, B. Zhu, S. Wang and S. Wu, *Sens. Actuators, B*, 2008, **131**, 183–189.
38 A. I. Ayesh, M. A. Haija, A. Shaheen and F. Bandat, *Appl. Phys. A*, 2017, **123**, 682–690.
39 J. Ma, L. Mei, Y. Chen, Q. Li, T. Wang, Z. Xu, X. Duan and W. Zheng, *Nanoscale*, 2013, **5**, 895–898.
40 Z. Sun, H. Yuan, Z. Liu, B. Han and X. Zhang, *Adv. Mater.*, 2005, **17**, 2993–2997.
41 Z. Jiang, J. Li, H. Aslan, Q. Li, Y. Li, M. Chen, Y. Huang, J. P. Froning, M. Otyepka, R. Zboril, F. Besenbacher and M. Dong, *J. Mater. Chem. A*, 2014, **2**, 6714.
42 Y. Wang, Y. Wang, J. Cao, F. Kong, H. Xia, J. Zhang, B. Zhu, S. Wang and S. Wu, *Sens. Actuators, B*, 2008, **131**, 183–189.
43 J. S. Lee, J. Oh, S. G. Kim and J. Jang, *Small*, 2015, **11**, 2399–2406.
44 S. Cho, J. S. Lee, J. Jun, S. G. Kim and J. Jang, *Nanoscale*, 2014, **6**, 15181–15195.